Channeling of spin waves in antiferromagnetic domain walls

Hyeon-Kyu Park and Sang-Koog Kim [*]

National Creative Research Initiative Center for Spin Dynamics and Spin-Wave Devices, Nanospinics Laboratory, Research Institute of Advanced Materials, Department of Materials Science and Engineering, Seoul National University, Seoul 151-744, South Korea

We theoretically calculated ultrafast propagations of spin waves channeled in antiferromagnetic Bloch-type domain walls based on a phenomenological theory developed by Hals *et al.* [Phys. Rev. Lett. **106**, 107206 (2011)]. Our analytical derivation demonstrates that the dispersion relation of such channeled spin waves exhibits an extremely high group velocity, up to $\sim$18.7 km/s, without any forbidden gap. Further, such electromagnetic-wave-like dispersion relation allows for dispersionless and translational transmission of trains of low-frequency, long-wavelength digital signals in the channel. Our results offer guidelines for the development of ultrafast information signal processing in nanoscale magnonic circuits composed of antiferromagnetic domain walls.

I. INTRODUCTION

Antiferromagnets are novel magnetic materials composed of sublattices of antiferromagnetically coupled spins that result in zero net magnetization. Most common antiferromagnetic materials (e.g., MnF_2, NiO, and $FeBO_3$) are composed of two sublattices that are ordered according to the staggered Néel order at sufficiently low temperature [1]. It was found that Néel orders of antiferromagnets are controllable via optical switching [2–4], which enables facile formation of metastable magnetic textures such as domain walls and skyrmions. The dynamics of antiferromagnetic domain walls is known to be much faster than that of their ferromagnetic counterparts, owing to the interatomic transfer of angular momentum within the spin system [5–7]. Also, the absence of the skyrmion Hall effect in antiferromagnets enables unidirectional current-driven motion of antiferromagnetic skyrmions [8,9]. These features make antiferromagnets a promising alternative to ferromagnets in the field of spintronics.

Spin waves, on the other hand, are small deviations in local magnetizations that coherently propagate across magnetic media. Optically excited spin waves in antiferromagnets show their resonant modes in the terahertz regime [10–12], and thus allow for faster operation of spin-wave devices [13] than do their ferromagnetic counterparts. The spin-wave dynamics of atomistic antiferromagnets, in the absence of uniaxial magnetic anisotropy, is captured by a simple pictorial model's linear dispersion law ($\omega \propto k$) [14]. More concrete forms of dispersion law for spin waves in antiferromagnets are posited in a phenomenological theory developed by Hals *et al.* [15] for a two-sublattice antiferromagnetic continuum. In the absence of externally applied magnetic fields, the dispersion of spin waves for antiferromagnets in a uniform state with uniaxial magnetic anisotropy along the z axis is given by the solution of the Klein-Gordon equation $\omega = \frac{\gamma}{M_S}\sqrt{a(Ak^2 + K_z)}$, where γ is the gyromagnetic ratio, M_S is the saturation magnetization, a is a homogeneous exchange constant, A is the exchange

stiffness, and K_z is the uniaxial magnetic anisotropy [5,16]. A few conclusions can be derived from this. First, the group velocity of spin waves in antiferromagnets is impeded by the presence of uniaxial magnetic anisotropy, which manifests in many antiferromagnetic materials such as MnF_2 [17,18] and FeF_2 [19]. Second, those spin waves must overcome a forbidden frequency gap of $\omega_{\text{gap}} = \frac{\gamma\sqrt{aK_z}}{M_S}$ in order to be excited. To enhance the group velocity of spin waves as well as to eradicate the forbidden gap, the channeling of spin waves inside domain walls has been proposed as an alternative to the reduction of uniaxial anisotropy itself in the case of ferromagnets [20]. Since Winter's original prediction of spin-wave channeling in domain walls [21], both theoretical [20,22–24] and experimental [25,26] studies have enhanced its efficiency and value by confining spin waves to reconfigurable domain wall composed curved paths.

Here, we explored the robust dynamics of spin waves' propagation in antiferromagnetic Bloch-type domain walls, as analytically derived based on a phenomenological theory for a two-sublattice antiferromagnet within the exchange approximation [15] and as further confirmed by micromagnetic simulations. In the case of ferromagnets, a gapless quasilinear dispersion relation for wall-bound spin-wave modes hosted by a Bloch-type domain wall is predicted [20]. In contrast to the ferromagnetic case, we found that the spin-wave modes hosted by an antiferromagnetic domain wall have much simpler dispersion relations due to the absence of dipolar volume charges. This dispersion relation resembles that of electromagnetic waves, enabling transmission of a binary digital signal (composed of trains of pulsed signals) resulting thereby in the concept of "digital magnonics" as an analog to conventional digital electronics. We demonstrated the dispersionless and translational transmission of a train of several pulses generated by a sinusoidal magnetic field over the course of half a period.

II. THEORY

We considered a two-dimensional ultrathin antiferromagnetic nanostrip, the longitudinal axis of which is placed on the

---

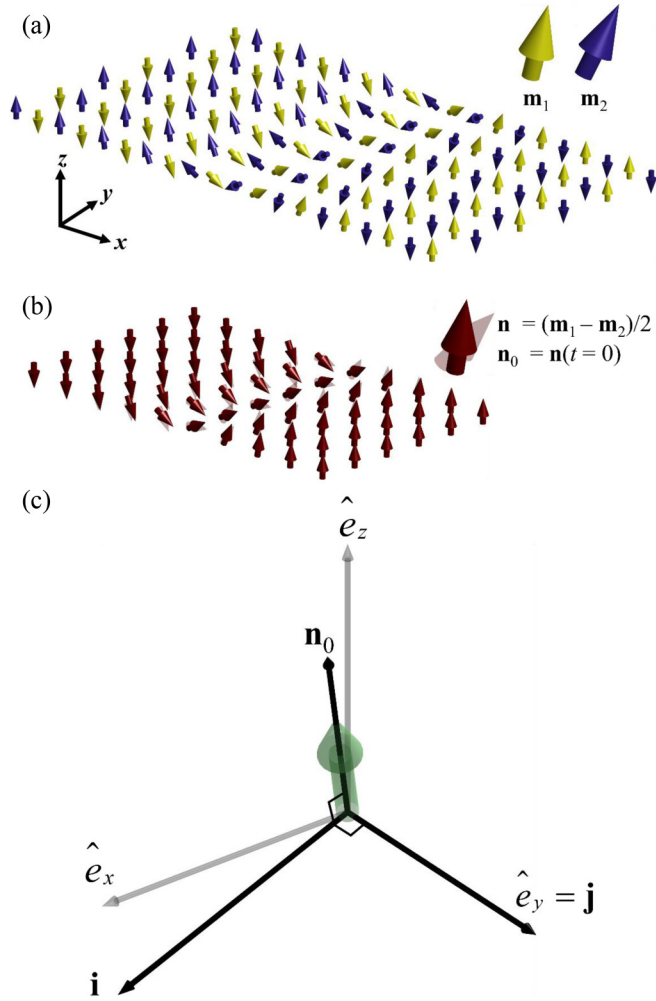*Corresponding author: sangkoog@snu.ac.kr

FIG. 1. Schematics of antiferromagnetic system considered in this work. (a) Toy model of antiferromagnetic domain walls of Bloch type. Each of the differently colored arrows corresponds to an atomistic magnetic moment on each sublattice of the bipartite antiferromagnets. (b) Toy model of antiferromagnetic domain walls represented in terms of Néel vector $\mathbf{n}$ ($=\frac{\mathbf{m}_1-\mathbf{m}_2}{2}$). Small deviations of Néel vectors that propagate along a specific direction are called spin waves (indicated as transparent arrows). (c) Coordinate system considered in this work. The transparent thin arrows indicate a conventional Cartesian coordinate system composed of $\hat{e}_x$, $\hat{e}_y$, and $\hat{e}_z$. The transparent green thick arrow at the center indicates the Néel vector in its ground state, $\mathbf{n}_0$. With respect to $\mathbf{n}_0$ and $\mathbf{j} = \hat{e}_y$, $\mathbf{i}$ is chosen such that $\mathbf{i} = \mathbf{j} \times \mathbf{n}_0$.

x axis under no external magnetic field. In Fig. 1(a), a model of antiferromagnetic domain walls of the Bloch type is illustrated with two-color arrows indicating two different magnetizations (unit vectors $\mathbf{m}_1$ and $\mathbf{m}_2$) on each sublattice. Once represented by the Néel order ($\mathbf{n} = \frac{\mathbf{m}_1-\mathbf{m}_2}{2}$), the antiferromagnetic domain wall can be considered to be in the same configuration as that of its ferromagnetic counterpart, as illustrated in Fig. 1(b). The antiferromagnetic domain wall separates two domains of upward and downward Néel orders. Since we assume a single monolayer lattice in the model, we can ignore spin-wave excitations along the z axis. The free energy of this system,

which is composed of a bipartite antiferromagnetic material with an isotropic exchange stiffness A and a uniaxial magnetic anisotropy K_z, is given as [15]

$$F = \int \frac{a}{2}\mathbf{m}^2 + \frac{A}{2}\sum_{i=x,y,z}(\partial_i\mathbf{n})^2 - \frac{K_z}{2}(\mathbf{n}\cdot\hat{z})^2 dV,$$

which is expressed in terms of the staggered Néel vector $\mathbf{n} = \frac{\mathbf{m}_1-\mathbf{m}_2}{2}$ and the averaged magnetization field $\mathbf{m} = \frac{\mathbf{m}_1+\mathbf{m}_2}{2}$. In the static state, the conditions $\mathbf{m}_1 = -\mathbf{m}_2$ and $\mathbf{m} = 0$ lead to the free energy $F_{\text{static}} = \int \frac{A}{2}\sum_{i=x,y,z}(\partial_i\mathbf{n})^2 - \frac{K_z}{2}(\mathbf{n}\cdot\hat{z})^2 dV$. The fields $\mathbf{n}$ and $\mathbf{m}$ are further constrained to obey $\mathbf{n}\cdot\mathbf{m} = 0$ and $\mathbf{n}^2 = 1$. The dynamic governing equations proposed by Hals *et al.* are given as $\dot{\mathbf{n}} = (\gamma\mu_0\mathbf{f}_m - G_1\dot{\mathbf{m}})\times\mathbf{n}$ and $\dot{\mathbf{m}} = (\gamma\mu_0\mathbf{f}_n - G_2\dot{\mathbf{n}})\times\mathbf{n} + (\gamma\mu_0\mathbf{f}_m - G_1\dot{\mathbf{m}})\times\mathbf{m}$, where γ is the effective gyromagnetic ratio; μ_0 is the vacuum permeability; G_1 and G_2 are dimensionless damping constants, which are arithmetic combinations of the Gilbert damping constant of each sublattice [27]; and $\mathbf{f}_n$ and $\mathbf{f}_m$ are the effective fields associated with $\mathbf{n}$ and $\mathbf{m}$, respectively. The variation of the free energy with the aid of suitable Lagrangian multipliers subject to the aforementioned constraints leads to $\mathbf{f}_m = -\frac{1}{\mu_0 M_S}\frac{\delta F}{\delta\mathbf{m}} = -\frac{a}{\mu_0 M_S}\mathbf{m}$ and $\mathbf{f}_n = -\frac{1}{\mu_0 M_S}\frac{\delta F}{\delta\mathbf{n}} = \frac{A}{\mu_0 M_S}\mathbf{n}\times(\nabla^2\mathbf{n}\times\mathbf{n}) + \frac{K_z}{\mu_0 M_S}(\mathbf{n}\cdot\hat{z})\mathbf{n}\times(\hat{z}\times\mathbf{n})$. Those equations would yield the same results even if the two sublattices were exchanged [15].

To find appropriate spin-wave solutions, we neglect the damping terms and linearize the equations given above by considering small variations around the ground Néel vector $\mathbf{n} = \mathbf{n}_0(\mathbf{x}) + \delta\mathbf{n}(\mathbf{x}, t)$ with $\mathbf{n}_0 = \mathbf{n}(\mathbf{x}, 0)$ and the averaged magnetization field $\mathbf{m} = \mathbf{m}(\mathbf{x}, t)$. Then, the first-order equations are given as [16]

$$\frac{M_S}{\gamma}\delta\dot{\mathbf{n}} = -a\mathbf{m}\times\mathbf{n}_0,$$

$$\frac{M_S}{\gamma}\dot{\mathbf{m}} = A(\nabla^2\mathbf{n}_0\times\mathbf{n}_0 + \nabla^2\delta\mathbf{n}\times\mathbf{n}_0 + \nabla^2\mathbf{n}_0\times\delta\mathbf{n})$$

$$+ K_z[(\mathbf{n}_0\cdot\hat{z})\hat{z}\times\mathbf{n} + (\delta\mathbf{n}\cdot\hat{z})\hat{z}\times\mathbf{n}_0].$$

Now, we assume a Bloch-type domain-wall profile in the system. In the case of Néel-type domain walls, a similar derivation can be obtained by permutation between the x and y coordinates. We introduce Walker's Bloch-type domain-wall profile centered along $y = 0$, i.e., $\mathbf{n}_0 = [\text{sech}(\frac{y}{\Delta}), 0, \tanh(\frac{y}{\Delta})]$, with the characteristic length of domain walls $\Delta = \sqrt{A/K_z}$, which minimizes the free energy of this system in the static state, $F_{\text{static}} = \int \frac{A}{2}\sum_{i=x,y,z}(\partial_i\mathbf{n})^2 - \frac{K_z}{2}(\mathbf{n}\cdot\hat{z})^2 dV$. We also make use of monochromatic waves, $\delta\mathbf{n} = [n_i(y)\mathbf{i} + n_j(y)\mathbf{j}]e^{i\omega t - i\mathbf{k}\cdot\mathbf{x}}$ and $\mathbf{m} = (m_i(y)\mathbf{i} + m_j(y)\mathbf{j})e^{i\omega t - i\mathbf{k}\cdot\mathbf{x}}$. In the expression, we use spatially smoothly varying and mutually orthogonal basis vectors $\mathbf{i}$ and $\mathbf{j}$ in order to express the fluctuating fields $\delta\mathbf{n}$ and $\mathbf{m}$ in the plane perpendicular to $\mathbf{n}_0$. As illustrated in Fig. 1(c), we choose to transform the coordinates with $\mathbf{j} = [0, 1, 0]$ and $\mathbf{i} = \mathbf{j}\times\mathbf{n}_0 = [\tanh(\frac{y}{\Delta}), 0, -\text{sech}(\frac{y}{\Delta})]$ for the sake of calculation simplicity.

Here, we assume that the spin waves are propagating along the x axis, i.e., $k_x = k$. By arranging the resultant equations on

the basis of **i** and **j**, we obtain

$$\frac{i\omega M_S}{\gamma}n_i = -am_j, \tag{1}$$

$$\frac{i\omega M_S}{\gamma}n_j = am_i, \tag{2}$$

$$\frac{i\omega M_S}{\gamma}m_i$$
$$= A\frac{d^2 n_j}{dy^2} - Ak^2 n_j + K_z\left[\text{sech}^2\left(\frac{y}{\Delta}\right) - \tanh^2\left(\frac{y}{\Delta}\right)\right]n_j, \tag{3}$$

$$\frac{i\omega M_S}{\gamma}m_j$$
$$= -A\frac{d^2 n_i}{dy^2} + Ak^2 n_i + K_z\left[\tanh^2\left(\frac{y}{\Delta}\right) - \text{sech}^2\left(\frac{y}{\Delta}\right)\right]n_i. \tag{4}$$

Equations (1) and (2) describe the dynamics of small variations around the ground Néel vector, $\delta\mathbf{n}$, in the **i** and **j** directions, respectively, while Eqs. (3) and (4) correspond to the dynamics of the canted magnetization **m** in the **i** and **j** directions, respectively. The dispersion relations for each pair of (n_i, m_j) and (n_j, m_i) components were obtained by coupling Eq. (1) to Eq. (4), and Eq. (2) to Eq. (3).

Now, there exist various virtual sets of solutions according to the spatial profiles of n_i and n_j, and their second spatial derivatives, $\frac{d^2 n_i}{dy^2}$ and $\frac{d^2 n_j}{dy^2}$. However, for the conditions $\omega = 0$ and $k = 0$, the pair of equations are expressed as $-\frac{d^2 n}{d\tilde{y}^2} + (\tanh^2 \tilde{y} - \text{sech}^2 \tilde{y}) = 0$ with $\tilde{y} = \frac{y}{\Delta}$. Thus, there exists a real-valued pair of solutions for both the (n_i, m_j) and (n_j, m_i) components, and they are wall-confined spin-wave modes [21],

$$n_i = K \text{sech}\left(\frac{y}{\Delta}\right), \quad m_j = L \text{sech}\left(\frac{y}{\Delta}\right), \tag{5a}$$

and

$$n_j = M \text{sech}\left(\frac{y}{\Delta}\right), \quad m_i = N \text{sech}\left(\frac{y}{\Delta}\right), \tag{5b}$$

with the dispersion relation $\omega = \frac{\gamma}{M_S}\sqrt{aAk^2}$, where K, L, M, and N are constants.

The dispersion relation for spin waves channeled in antiferromagnetic domain walls is even simpler than that for spin waves channeled in ferromagnetic ones [20,28], due to the absence of dipolar volume charges. Also, the dispersion relation resembles that obtained from the Klein-Gordon equation without a mass, but the concomitant spin waves rather have a hyperbolic secant cross-sectional profile. Along the x axis, n_i and n_j correspond to $-\delta n_z(=-\delta\mathbf{n}\cdot\hat{z})$ and $\delta n_y(=\delta\mathbf{n}\cdot\hat{y})$, and m_i and m_j correspond to $-m_z$ and m_y in Cartesian coordinates, respectively. Thus, the δn_z and m_y (or δn_y and m_z) components must obey the gapless dispersion law as given by $\omega = \frac{\gamma}{M_S}\sqrt{aAk^2}$.

Figure 2 shows a plot of the above dispersion equation (blue solid line) using a set of material parameters accordant with MnF$_2$ ($a = 2.67 \times 10^8$ J/m^3, $A = 9.32 \times 10^{-12}$ J/m, $M_S = 4.71 \times 10^5$ A/m, and $K_z = 3.92 \times 10^5$ J/m^3) [17,29], as compared with the dispersion relation in a uniform state (blue dashed line). The dispersion of $\omega = \frac{\gamma}{M_S}\sqrt{aAk^2}$ allows
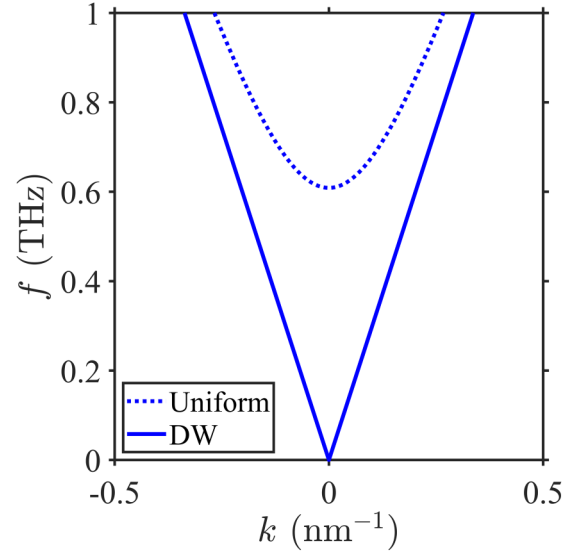

FIG. 2. Comparison between dispersion relations for spin waves in antiferromagnets with different metastable states. The blue solid line indicates the dispersion relation for spin waves channeled in antiferromagnetic domain walls, while the blue dashed line indicates the dispersion relation for spin waves in antiferromagnets with uniform Néel vectors.

for a maximum possible group velocity, which, in the case of a uniform state, is asymptotically approachable only at an infinite frequency. For a specific antiferromagnet of MnF$_2$ with the material parameters given in Refs. [17,29] along with the gyromagnetic ratio of a free electron, the group velocity is estimated to be ~18.7 km/s, which is one order of magnitude higher than that for ferromagnetic permalloy both in the uniform state and in domain walls (1.0–3.5 km/s) [20,24,30,31]. Such gapless dispersion for spin waves channeled in antiferromagnetic domain walls allows for high group velocities even in long-wavelength and low-frequency regimes. This feature allows for lower power dissipation [$P = (G_1/\gamma)\dot{\mathbf{m}}^2 + (G_2/\gamma)\dot{\mathbf{n}}^2$] that is proportional to the square of frequency [15] as well as employment of transistor circuits in a high-gain regime.

III. NUMERICAL SIMULATION

According to the above analytical prediction, in order to confirm the validity of such high group velocity in the long-wavelength regime, we conducted numerical simulations of spin waves channeled in antiferromagnetic domain walls. The model system is an ultrathin nanostrip of 41 nm width, 401 nm length, and monolayer thickness, as shown in Fig. 3(a). The cell size used is 1 nm × 1 nm. Since the strip is as thin as 0.33 nm [18], we assumed nonexcitation of spin waves along the thickness (z axis). The initial magnetization state [Fig. 3(a)] was obtained by relaxation with a Bloch-type domain-wall configuration for the sufficiently long time of 5.0 ns. In the simulation, the total free energy F with respect to a perturbative magnetic field **H** was given as

$$F = \int \frac{a}{2}\mathbf{m}^2 + \frac{A}{2}\sum_{i=x,y,z}(\partial_i \mathbf{n})^2 - \frac{K_z}{2}(\mathbf{n}\cdot\hat{z})^2 - \mu_0 M_S\mathbf{H}\cdot\mathbf{m}\,dV,$$
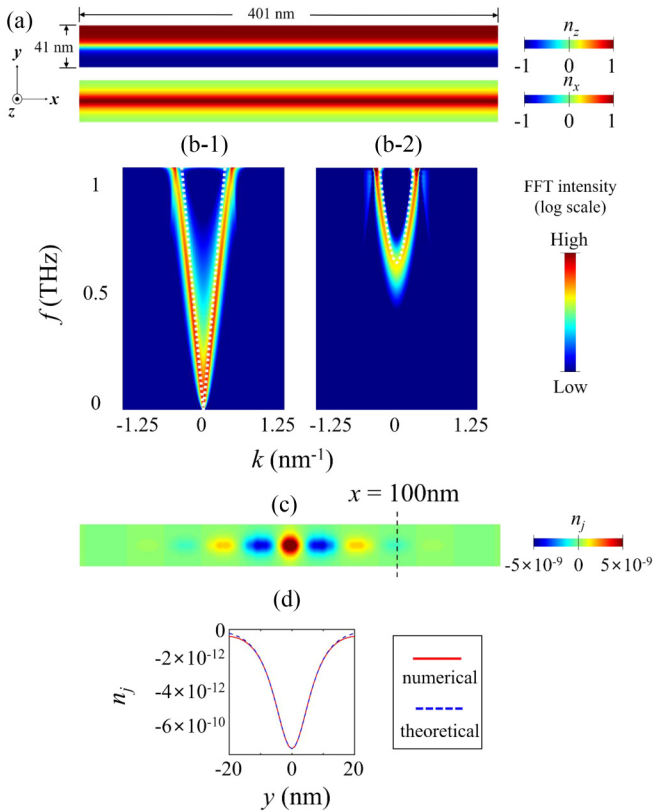
FIG. 3. Spin-wave excitations along straight antiferromagnetic domain wall. (a) Néel-vector configurations of components n_z and n_x in the metastable ground state. Such Néel-vector configurations locally minimize the free energy in the static state, $F_{static} = \int \frac{A}{2} \sum_i (\partial_i \mathbf{n})^2 - \frac{K_z}{2} (\mathbf{n} \cdot \hat{z})^2 dV$. (b-1) Dispersion relation for spin waves channeled in antiferromagnetic domain wall of Bloch type. The white dotted lines denote the analytically derived dispersion relation, $\omega = \frac{\gamma}{M_S} \sqrt{aAk^2}$. (b-2) Dispersion relation for spin waves traveling longitudinally in uniformly magnetized antiferromagnet. (c) Temporal spatial profile of spin-wave component of n_j, obtained by inverse Fourier transform at frequency of 0.25 THz. The spin waves are well channeled in the domain wall. (d) Cross-sectional spin-wave profile at $x = 100$ nm (red lines) and numerically calculated hyperbolic secant profile (blue dotted lines).

where $a = 4zJS^2/l^3$, $A = zJS^2/2l$, and $K_z = 2DS^2/l^3$ in terms of coordinate number z, lattice parameter l, the number of spins per atom S, exchange energy J, and anisotropy energy D [16–18,29]. The first, second, third, and last terms correspond to homogeneous exchange energy, inhomogeneous exchange energy, uniaxial anisotropy energy, and Zeeman energy, respectively. Under this condition, the effective fields $\mathbf{f}_m$ and $\mathbf{f}_n$ become $\mathbf{f}_m = -\frac{a}{\mu_0 M_S} \mathbf{m} + \mathbf{n} \times (\mathbf{H} \times \mathbf{n})$ and $\mathbf{f}_n = \frac{A}{\mu_0 M_S} \mathbf{n} \times (\nabla^2 \mathbf{n} \times \mathbf{n}) + \frac{K_z}{\mu_0 M_S} (\mathbf{n} \cdot \hat{z}) \mathbf{n} \times (\hat{z} \times \mathbf{n}) - (\mathbf{n} \cdot \mathbf{H}) \mathbf{m}$. To compare the simulation and analytical calculations, we used material parameters corresponding to the G-type antiferromagnet MnF_2 of a rutile structure ($a = 2.67 \times 10^8$ J/m^3, $A = 9.32 \times 10^{-12}$ J/m, $M_S = 4.71 \times 10^5$ A/m, and $K_z = 3.92 \times 10^5$ J/m^3) along with the gyromagnetic ratio of free electrons [17,29]. In order to excite a number of spin waves with different frequencies at once, we applied a nonharmonic sinc-function magnetic field,

$\mathbf{H} = H_0 \frac{\sin[2\pi f(t-t_0)]}{2\pi f(t-t_0)} \hat{z}$ ($t_0 = 0.5$ ps, $f = 1$ THz, $H_0 = 10$ Oe), to a central region of 41 nm × 1 nm.

With the functional derivatives and $\mathbf{H}$ plugged into the effective field terms, we integrated the resultant equations by the fourth-order Runge-Kutta method. The resultant dispersion obtained from the fast Fourier transform (FFT) of the excitation of the Néel-vector field n_j is given in the left side of Fig. 3(b). The numerical simulation agrees well with the analytical derivation, $\omega = \frac{\gamma}{M_S} \sqrt{aAk^2}$, marked by the white dotted line. An FFT of the canted magnetization mi, which is directly coupled to nj according to Eqs. (2) and (3), also displayed a dispersion relation like this [32]. We additionally compared the dispersion curve obtained from the FFTs of the mx oscillations in a uniformly magnetized nanostrip, along with the analytical form of $\omega = \frac{\gamma}{M_S} \sqrt{a(Ak^2 + K_z)}$ marked by the white dotted line, as shown in the right side of Fig. 3(b). In order to verify the spin-wave propagations along the Bloch-type domain wall, the temporal profiles of n_j were obtained by inverse FFTs at a specific frequency of 0.25 THz [Fig. 3(c)]. The cross-sectional spin-wave profiles (red line) along the y axis at the specific position of $x = 100$ nm also are shown in Fig. 3(d), whose result agrees well with the analytical derivation (blue dashed line), $K \operatorname{sech}(\frac{y}{\Delta})$ and $L \operatorname{sech}(\frac{y}{\Delta})$. Channeling of spin waves with hyperbolic secant profiles was well demonstrated at other frequencies [32]. Experimentally, the presence of those bound spin waves can be demonstrated with the help of a three-magnon scattering process [33,34] through which one can analyze magnonic excitations in order to detect abnormal frequency peaks using time-resolved optical techniques [35]. One interesting consequence of such linear dispersion relation of spin waves channeled in an antiferromagnetic domain wall is that the phase and group velocity are equivalent to a constant value of $\frac{\gamma}{M_S} \sqrt{aA}$ in any frequency regime, leading to a dispersionless transmission of pulsed signals, just like an electromagnetic wave (or a light) in a vacuum. This means that in the antiferromagnetic domain wall, all frequencies have the same group velocity.

From an application point of view, such gapless linear dispersion offers a great benefit to implementation of the transmission of binary (or multilevel) digital signals in the form of trains of pulsed signals as in digital electronics along with lower power consumption. In digital magnonics, spin waves in antiferromagnetic domain walls are transmitted in the form of pulsed signals encoding binary digits without Joule heating and with long coherence length. One example of the propagation of pulsed signals channeled in antiferromagnetic domain walls is shown in Fig. 4(a). We used the same geometry as in Fig. 3(a) and neglected the damping parameters in order to prevent the pulses from attenuating. The pulses were generated with a field pulse in the central region (41 nm × 1 nm) composed of a sinusoidal oscillation, $\mathbf{H}_p = H_{p,0} \sin(2\pi f_p t)\hat{z}$ ($f_p = 0.8$ THz, $H_{p,0} = 10$ Oe) over half a period. The temporal evolution of the n_y component of the pulsed signal is shown for three instant times after the application of the pulsed field. Over 6 ps, the pulsed signals only underwent a dispersionless, translational motion, because every contribution of spin waves with different wave numbers translated according to the same phase velocity, $\frac{\gamma}{M_S} \sqrt{aA}$. That is, the pulsed signal n_y can be written
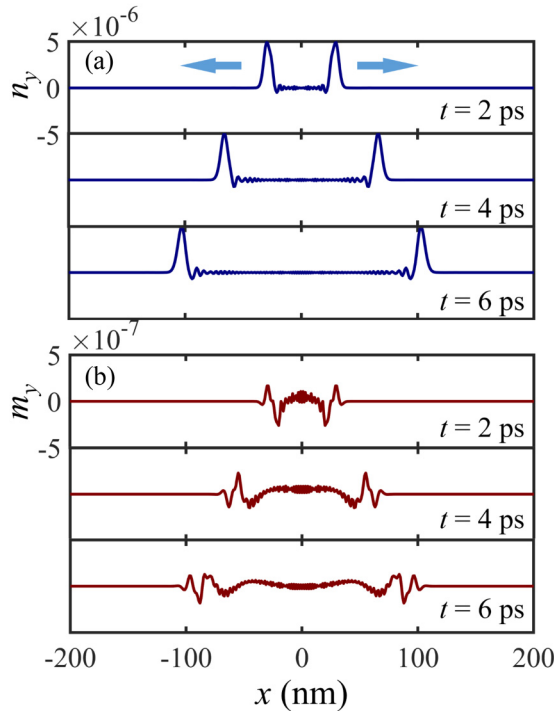
FIG. 4. Temporal variation of (a) n_y component of pulsed spin waves in antiferromagnetic domain wall and (b) m_y component of pulsed spin waves in uniform antiferromagnet shown at three instant times of $t = 2$ ps, $t = 4$ ps, and $t = 6$ ps. The pulsed spin waves propagate (a) without dispersion in the antiferromagnetic domain wall and (b) with considerable dispersion in the uniform antiferromagnet.

$n_y(x, t) = \sum_\omega \sum_k \hat{n}_y(\omega, k) e^{i\omega t - ikx}$, where $\hat{n}_y(\omega, k) e^{i\omega t - ikx}$ is the contribution of n_y from harmonic waves of frequency ω and wave number k, and their phase velocity is $|v_p| = |\frac{\omega}{k}| = \frac{\gamma}{M_S}\sqrt{aA}$. The average group velocity of the pulse was 18.1 km/s, close to the analytical derivation of 18.7 km/s. Based on this idea, we provide an example application of digital-signal transmission along an antiferromagnetic domain-wall channel in the Supplemental Material S3 [32]. For compari-son, we also simulated the temporal evolution of spin-wave pulses in an assumed uniform antiferromagnet in the right side of Fig. 3(b). The damping parameters were neglected in this case as well, and the applied pulsed field was $\mathbf{H}_p = H_{p,0} \sin(2\pi f_p t)\hat{y}$ ($f_p = 0.8$ THz, $H_{p,0} = 10$ Oe) over half a period. As seen from the three instant times after application of the pulsed magnetic fields [Fig. 4(b)], the pulsed signals in the uniform antiferromagnets showed a significant dispersion, since each contribution of m_y had different phase velocities at different ω and k values.

IV. CONCLUSION

In conclusion, we developed a theory of the dispersion of spin waves propagating in an antiferromagnetic domain wall. By assuming that the metastable static magnetization is aligned in Walker's profile, we revealed that the dispersion is gapless with a constant group velocity in all frequencies, like light in a vacuum. Our derived dispersion relation allows for magnetic sources of very low frequency to excite long-wavelength spin waves. Since the propagation properties of spin waves channeled inside domain walls depend only on the intrinsic magnetic parameters, the coherence length for the spin waves propagating in domain walls is expected to sig-nificantly enhance that for spin waves in magnetic domains. Such longer coherence lengths are essential for realization of spin-wave logic gates that encode information in either the amplitude or the phase of spin waves. Moreover, transmis-sion of pulsed signals along antiferromagnetic domain-wall channels is expected to be applicable to digital magnonics, as binary pulse signals are typically generated by metal oxide semiconductor field-effect transistor (MOSFET) devices ow-ing to their rapid on-off switching behavior.

[1] A. Smerald, *Theory of the Nuclear Magnetic 1/T$_1$ Relaxation Rate in Conventional and Unconventional Magnets* (Springer, New York, 2013).

[2] S. Loth, S. Baumann, C. P. Lutz, D. M. Eigler, and A. J. Heinrich, Science **335**, 196 (2012).

[3] P. Němec, M. Fiebig, T. Kampfrath, and A. V. Kimel, Nat. Phys. **14**, 229 (2018).

[4] S. Manz, M. Matsubara, T. Lottermoser, J. Büchi, A. Iyama, T. Kimura, D. Meier, and M. Fiebig, Nat. Photon. **10**, 653 (2016).

[5] T. Shiino, S.-H. Oh, P. M. Haney, S.-W. Lee, G. Go, B.-G. Park, and K.-J. Lee, Phys. Rev. Lett. **117**, 087203 (2016).

[6] E. G. Tveten, A. Qaiumzadeh, and A. Brataas, Phys. Rev. Lett. **112**, 147204 (2014).

[7] N. Thielemann-Kühn, D. Schick, N. Pontius, C. Trabant, R. Mitzner, K. Holldack, H. Zabel, A. Föhlisch, and C. Schüßler-Langeheine, Phys. Rev. Lett. **119**, 197202 (2017).

[8] J. Barker and O. A. Tretiakov, Phys. Rev. Lett. **116**, 147203 (2016).

[9] X. Zhang, Y. Zhou, and M. Ezawa, Sci. Rep. **6**, 24795 (2016).

[10] T. Kampfrath, A. Sell, G. Klatt, A. Pashkin, S. Mährlein, T. Dekorsy, M. Wolf, M. Fiebig, A. Leitenstorfer, and R. Huber, Nat. Photon. **5**, 31 (2011).

[11] Q. Li, M. Yang, C. Klewe, P. Shafer, A. T. N'Diaye, D. Hou, T. Y. Wang, N. Gao, E. Saitoh, C. Hwang *et al.*, Nat. Commun. **10**, 5265 (2019).

[12] C. Tzschaschel, K. Otani, R. Iida, T. Shimura, H. Ueda, S. Günther, M. Fiebig, and T. Satoh, Phys. Rev. B **95**, 174407 (2017).

[13] R. Cheng, M. W. Daniels, J.-G. Zhu, and D. Xiao, Sci. Rep. **6**, 24223 (2016).

[14] F. Keffer, H. Kaplan, and Y. Yafet, Am. J. Phys. **21**, 250 (1953).

[15] K. M. D. Hals, Y. Tserkovnyak, and A. Brataas, Phys. Rev. Lett. **106**, 107206 (2011).

[16] R. E. Troncoso, C. Ulloa, F. Pesce, and A. S. Nunez, Phys. Rev. B **92**, 224424 (2015).

[17] F. Keffer, Phys. Rev. **87**, 608 (1952).

[18] J. Barak, V. Jaccarino, and S. M. Rezende, J. Magn. Magn. Mater. **9**, 323 (1978).

[19] J. W. Stout and L. M. Matarrese, Rev. Mod. Phys. **25**, 338 (1953).

[20] F. Garcia-Sanchez, P. Borys, R. Soucaille, J.-P. Adam, R. L. Stamps, and J.-V. Kim, Phys. Rev. Lett. **114**, 247206 (2015).

[21] J. M. Winter, Phys. Rev. **124**, 452 (1961).

[22] X. Xing and Y. Zhou, NPG Asia Mater. **8**, e246 (2016).

[23] Y. Henry, D. Stoeffler, J.-V. Kim, and M. Bailleul, Phys. Rev. B **100**, 024416 (2019).

[24] H.-K. Park, J.-H. Lee, J. Yang, and S.-K. Kim, J. Appl. Phys. **127**, 183906 (2020).

[25] K. Wagner, A. Kákay, K. Schultheiss, A. Henschke, T. Sebastian, and H. Schultheiss, Nat. Nanotechnol. **11**, 432 (2016).

[26] E. Albisetti, D. Petti, G. Sala, R. Silvani, S. Tacchi, S. Finizio, S. Wintz, A. Calò, X. Zheng, J. Raabe *et al.*, Commun. Phys. **1**, 56 (2018).

[27] A. Kamra, R. E. Troncoso, W. Belzig, and A. Brataas, Phys. Rev. B **98**, 184402 (2018).

[28] V. Sluka, T. Schneider, R. A. Gallardo, A. Kákay, M. Weigand, T. Warnatz, R. Mattheis, A. Roldán-Molina, P. Landeros, V. Tiberkevich *et al.*, Nat. Nanotechnol. **14**, 328 (2019).

[29] F. M. Johnson and A. H. Nethercot, Jr., Phys. Rev. **114**, 705 (1959).

[30] G. Duerr, K. Thurner, J. Topp, R. Huber, and D. Grundler, Phys. Rev. Lett. **108**, 227202 (2012).

[31] C. Liu, J. Chen, T. Liu, F. Heimbach, H. Yu, Y. Xiao, J. Hu, M. Liu, H. Chang, T. Stueckler *et al.*, Nat. Commun. **9**, 738 (2018).

[32] See Supplemental Material at http://link.aps.org/supplemental/10.1103/PhysRevB.103.214420 for more details on the numerical simulations and digital-signal transmission.

[33] B. Zhang, Z. Wang, Y. Cao, P. Yan, and X. R. Wang, Phys. Rev. B **97**, 094421 (2018).

[34] L. Körber, K. Schultheiss, T. Hula, R. Verba, J. Fassbender, A. Kákay, and H. Schultheiss, Phys. Rev. Lett. **125**, 207203 (2020).

[35] J. Yang, N. Pellatz, T. Wolf, R. Nandkishore, and D. Reznik, Nat. Commun. **11**, 2548 (2020).